ACS OMEGA

http://pubs.acs.org/journal/acsodf

Article

Synthesis and Growth Mechanism of SiS_2 Rods

Meng-Xiang Xie, Ji-Wei Zhang, Yong Zhang, Hou-Ran Wu, Yan-Pei Wang, Wen-Hao Wang, and Gang-Qin Shao*

Cite This: *ACS Omega* 2022, 7, 22500−22510

Read Online

ACCESS | Metrics & More | Article Recommendations | Supporting Information

ABSTRACT: The SiS_2 rods exhibit a significant anisotropy property applied in a special field such as in the one of all-solid-state lithium-ion batteries and so on. In this work, the orthorhombic SiS_2 rods with high chemical/phase purity were prepared by an elemental method, either through a boiling or a steaming process, at 1023−1073 K for 3 h and under the saturated S-vapor pressure (2.57−3.83 MPa) in a closed sealed-tube system. The composition, crystal structure, morphology, and growth mechanism were investigated. Results showed that the growth orientation of SiS_2 along the <0 0 1> is intrinsically governed by the crystal structure motif. It could exist in both processes and the latter tends to show in macroscopic morphology. Using the pressure-temperature diagram, structure refinement, pole figures, image analyses, and so forth, factors influencing the purity and growth of SiS_2 rods were concluded from the thermodynamics and kinetics viewpoints.

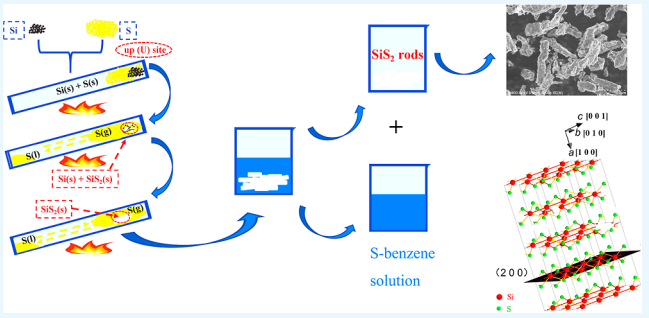

1. INTRODUCTION

Silicon disulfide (SiS_2) is an important synthetic compound used in fundamental and applied research. It is one of the important raw materials for sulfide-based solid electrolytes.[1−12] There are five polymorphs of SiS_2. One is the ambient-pressure (NP) phase (≤3.83 MPa, 973−1570 K)[10,11,13−18] with an orthorhombic structure (*Ibam*, Space Group no. 72), which can remain stable up to 6.9 GPa at RT.[10] The other four are high-pressure (HP) phases, while HP1-, HP2-, and HP3-phases are quenchable under ambient conditions. Monoclinic HP1-/HP2-phases ($P12_1/c1$, no. 14) form under 2.8/3.5 GPa at 1473 K, respectively. They have different unit-cells ($Z = 4$ vs $Z = 12$) and the c value of the former [5.8261(8) Å] is smaller than that of the latter [14.747(2) Å].[11] The tetragonal HP3-phase ($I\bar{4}2d$, no. 122) forms under 4.0−7.5 GPa at 1373−1703 K.[11,14,15] The trigonal HP4-phase ($P\bar{3}m1$, no. 164) cannot be obtained by quenching from a high temperature. It can only form through in situ high-pressing (27.5−29.6 GPa) at RT,[10] either from a stable NP-phase or one of the above three metastable HP-phases.

The SiS_2 has an extreme-high selling price due to its complex synthesis methods restrained by its sensitivity toward hydrolysis and oxidation to generate the toxic H_2S with a penetrating odor.[5,19]

Synthesis methods for NP-SiS_2 have been summarized[5] and classified into two groups: compound[3,13,16−20] and elemental[6,10,11,20−22] methods. As for the latter, both silicon (Si) and sulfur (S) sources are elementary substances. It has advantages of easy availability of raw materials, simple process, no environmental pollution, safety, and less corrosion of equipment. At present, the "elemental method" for NP-SiS_2 has become the main priority for academic research and scale production. The related reaction takes place at a certain temperature in a sealed quartz or quartz-lined steel container, similarly in a low-/medium-pressure hydrothermal kettle.

There are two routes in the "elemental method".

The first is with a dual-temperature zone having a temperature gradient between the cold- and hot-ends of the container.[10,11,20,21] The synthesis reaction happens at the hot-end. The S-vapor circulates between the two ends. The ambient reaction pressure (NP) depends on the saturated S-vapor pressure ($P_{sat.}$@S) at the cold-end rather than the pressure at the hot-end. This route ensures effectively the safe use of quartz tubes. However, it is at the expense of the reaction pressure reduction due to the lower cold-end temperature (vs hot-end temperature). The reaction time has to be extended. The requirement with a longer tube would decrease the effective reaction volume and therefore increase the equipment complexity and difficulty to use.

The second is with a uniform-temperature zone while the NP varies. When NP ≤ $P_{ctrl.}$, the reaction can take place safely ($P_{ctrl.}$—the control pressure set for safe use of quartz tubes; being equal to 3.83 MPa in this work).

Received: March 22, 2022
Accepted: June 8, 2022
Published: June 23, 2022

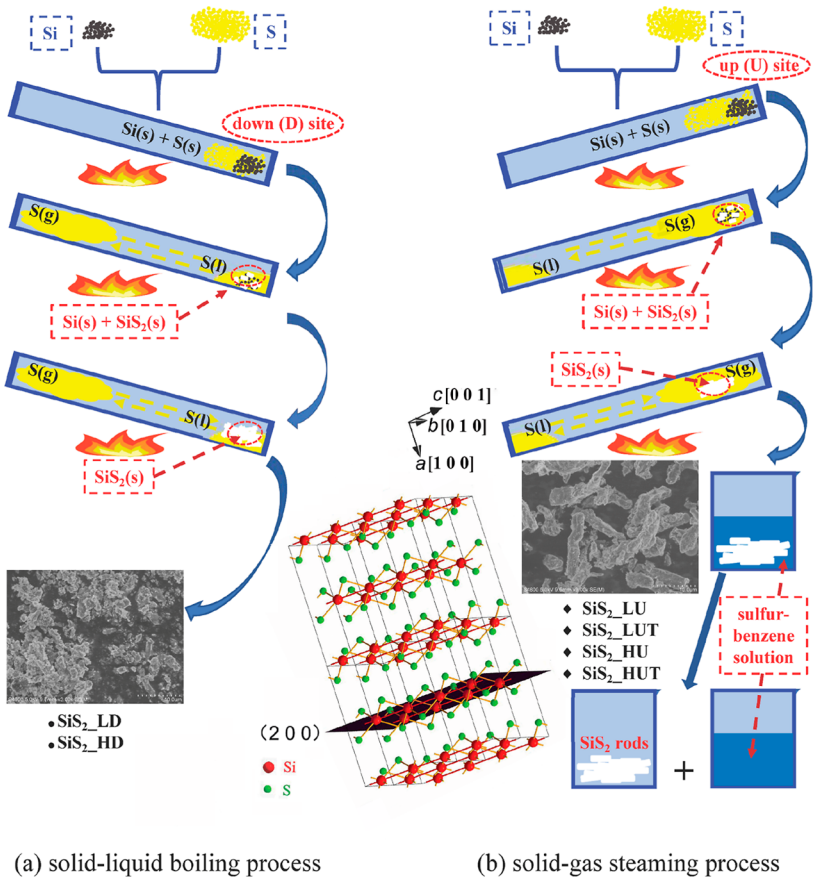

Figure 1. Preparation of the flow chart of SiS_2. (a) Solid−liquid boiling process; (b) solid−gas steaming process.

$$\mathrm{NP} = min[P_i@S,\ P_{ctrl.},\ P_{sat.}@S] = \begin{cases} P_{sat.}@S,\ \text{while } P_{sat.}@S \le P_i@S \ \&\ P_{sat.}@S \le P_{ctrl.} < P_{expl.}(\text{Block I}) \\ P_i@S,\ \text{while } P_i@S < P_{sat.}@S < P_{ctrl.} < P_{expl.}(\text{Block II}) \\ P_i@S,\ \text{while } P_i@S \le P_{ctrl.} < P_{sat.}@S < P_{expl.}(\text{Block III}) \end{cases} \quad (1)$$

where Blocks I−IV correspond to the four *P*-*T* relevant quadrants (labeled in Figure 2, see Section 2). The $P_i@S$ is the ideal gas pressure of S calculated by the ideal gas equation ($= n_S R T V_q^{-1}$, MPa), where $T > T_{b.p.}@S$ (717.75 K).[23] The n_S is the mole number of S, R is the ideal gas constant (8.3144 J·mol^{-1}·K^{-1}), and V_q is the active volume (dm^3). Next, the $P_{expl.}$ is the pressure limit of tube explosion. When NP > $P_{ctrl.}$ and meanwhile > $P_{expl.}$, quartz tubes would explode (Block IV). In practical application, the $P_{expl.}$ value of a commercially available quartz tube is about several megapascals (MPa), far below the tensile strength of a silica rod (~120 MPa at 923−1073 K).[24,25]

By using the uniform-temperature zone, it makes full use of the advantage of pressure increasing (thus enhancing reaction rate) caused by sulfur gasification.[5,6,21,22] Compared to the dual-temperature zone, the reaction temperature here is between that at the hot-end and the cold-end. Therefore, the reaction pressure in the uniform-temperature zone is higher than that in the dual-temperature zone, while the latter depends on the $P_{sat.}@S$ at the cold-end. The route via the uniform-temperature zone can improve the rate constant (k) and conversion rate (η) in an exothermic reaction, which is also applied in this work.

However, there remains still some challenges in the application of the "elemental method", e.g., low purity of SiS_2, set for the safe use of quartz tubes complicated process to eliminate residual S,[6] long production period (soaking for 150 h,[20] 3 d[10,11] or 7 d;[22] calcining for 70−80 h[6] or 12 d[10,11]), too many production procedures,[6] high-temperature/pressure safety problems,[5,6] and detailed growth kinetics of rods (*c.f.* CdS, ZnO, et al.).[26,27]

We prepared SiS_2 2 years before through an "elemental-synthesis gasifying separation" (ESGS) process.[5] This work is to reinvestigate/optimize the control techniques for solid−liquid/solid−gas reactions, chemical/phase-purity and microstructure of SiS_2. The chemical (*c.f.* evaporation) approach using benzene is first used to eliminate residual S to prepare pure SiS_2. The growth mechanism of SiS_2 rods is proposed.

2. MATERIALS AND CHARACTERIZATION

The preparation flow chart of SiS_2 is shown in Figure 1 and the ambient pressure (NP) via temperature (T) diagram for synthesizing SiS_2 in Figure 2.

S Powder. The commercially available S powder (99 wt %, Beijing Xinguang Chem. Reag. Fact., China) was washed first by aqua regia with a HCl/HNO_3 ratio of 3:1 (vol %) (36.0−38.0 wt % HCl, Shanghai Chem. Reag. Fact., China; 65.0−68.0 wt % HNO_3, Shanghai Chem. Reag. Fact., China). Then, it was washed many times with ultrapure water (>18 MΩ·cm), until no Cl^- could be detected in the washing solution and pH = 7. The

https://doi.org/10.1021/acsomega.2c01725
ACS Omega 2022, 7, 22500−22510

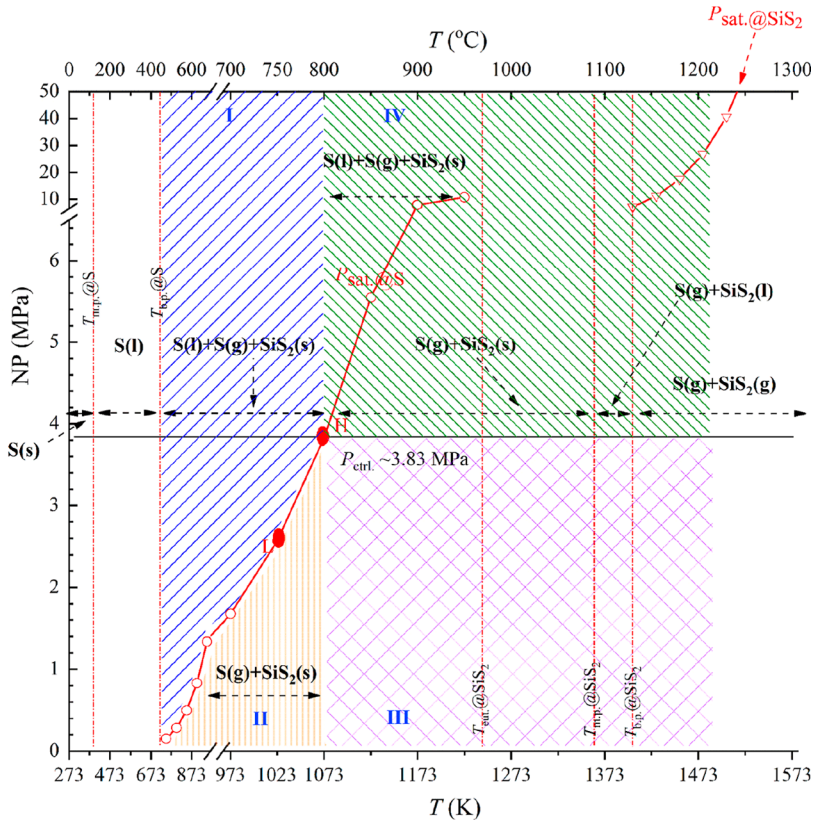

Figure 2. Ambient pressure (NP) via temperature (T) diagram for synthesizing SiS_2. $T_{m.p.}$@S—melting point of S (388.36 K);[23,32] $T_{b.p.}$@S—boiling point of S (717.75 K);[23,32] $T_{e.p.}$@SiS_2—eutectic point of SiS_2 (1240 K);[23] $T_{m.p.}$@SiS_2—melting point of SiS_2 (1363 K);[18,19,33] $T_{b.p.}$@SiS_2—boiling point of SiS_2 (1403 K);[19,33] $P_{sat.}$@S—saturated S-vapor pressure calculated from Rau et al.'s equation,[34] where $T_{b.p.}$@S < $T \leq T_{b.p.}$@SiS_2; and $P_{sat.}$@SiS_2—saturated SiS_2-vapor pressure calculated via HSC software, where $T > T_{b.p.}$@SiS_2.

washed substance was vacuum-dried and sieved through 200 mesh (<74 μm).

Si Powder. A certain number of polysilicon blocks (7N, Xinte Energy Co. Ltd., China) were broken and put into a stainless-steel vessel, together with Fe-balls (ϕ5.9 mm) and ethanol (99.7 wt %, Shanghai Chem. Reag. Fact., China) at the ratio of 1 (Si): 8 (Fe-balls): 1 (ethanol) (wt %). Ball-milling proceeded for 12 h at 150 rpm for revolution and 300 rpm for rotation in a planetary mill (QM-DY9, Nanjing Instr. Fact., China). The Si slurry was washed in sequence by 10 wt % HCl and 6 wt % HF (≥40.0 wt %, Shanghai Chem. Reag. Fact., China). Then, it was washed with ultrapure water and ethanol and vacuum-dried and sieved as the above. The Teflon utensils and containers were used when HF was involved in experiments. As a comparison, some Si powder was prepared by using WC-Co balls (ϕ6.1 mm) for 2 h. Then, the Fe-ball-milled Si powder was denoted as "Si" and the WC-Co-ball-milled Si powder was denoted as "Si$^{\#}$".

SiS_2 Powder. The obtained S and Si powders were mixed at the mole ratio (δ) of 3.3 : 1, that is, δ = 3.3, and then sealed in quartz tubes and vacuumed to 10 Pa with Ar. Each tube (V_q = 0.0121 dm^3) contains 2 g of powder, equivalent to that m_{Si} = 34.6 g/dm^3. At least three tubes were used for one sample. Quartz tubes were laid diagonally in the furnace at a certain angle of 15°−25°. Half of them contained reactants at a down (D) site (for the solid−liquid boiling process; Figure 1a) and the other half at an up (U) site (for the solid−gas steaming process; Figure 1b). Samples were heated at low (L) or high (H) temperature (1023/1073 K) for 3 h then cooled down to RT. Both heating and cooling rates were 5 °C/min. Products were taken out by cutting quartz tubes and then treated (T) with benzene (Sinopharm, China; ≥ 99.5 wt %) in an Ar-filled glovebox (H_2O < 0.1 ppm, O_2 < 0.1 ppm). Last, they were vacuum-dried and sieved through 200 mesh (<74 μm).[5,28,29] For the following reasons, benzene was used in this work—It is the simplest aromatic hydrocarbon with a stable ring connected by delocalized big π-bonds. The hydrogen atoms on the ring are easy to be replaced but difficult to react with the oxygen in air (at RT). Addition reactions are difficult to proceed while it is used. It does not dissolve or react with the target product SiS_2. However, it can dissolve residual S and other impurities.[30]

Samples were labeled hereafter with suffixes such as H, L, U, D, and T to represent those prepared at different conditions, for example, SiS_2_HUT refers to the SiS_2 prepared at a high (H) temperature of 1073 K, while the quartz tube was at an up (U) site, and treated (T) by benzene.

Chemical compositions were analyzed by an inductively coupled plasma-optical emission spectrometer (ICP Prodigy 7, Leeman Labs Inc., USA). The crystal structure and phase purity were determined by X-ray powder diffraction (XRD) using CuK_α radiation ($\lambda_{\alpha 1}$ = 1.54060 Å, 40 kV, 40 mA) in a flat plate θ/2θ geometry with a step size of 0.01313°/step and a time per step of 128.52 s/step (Empyrean, PANalytical B.V., Netherlands). Samples were protected from water and oxygen through a special sample stage (Deen Optics Co., China) with shielding Ar in Kapton tapes.

The structure refinement with spherical harmonics function was performed by the Rietveld method implemented in GSAS/

https://doi.org/10.1021/acsomega.2c01725
ACS Omega 2022, 7, 22500−22510

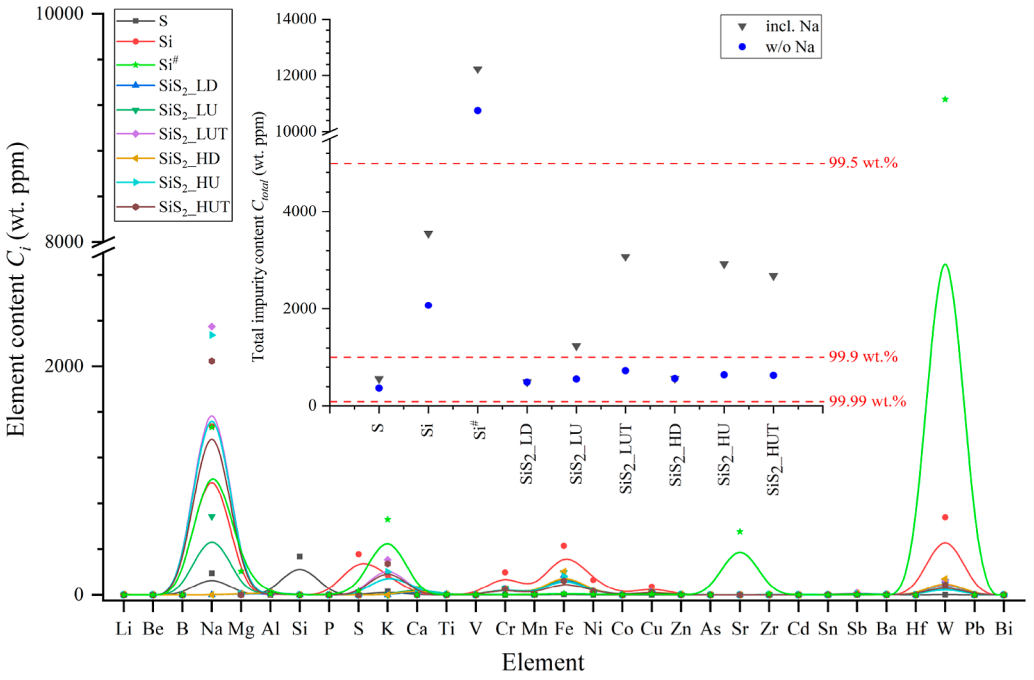

Figure 3. ICP analysis results of the acid-pickled raw materials (S, Si, and Si#) and the synthesized SiS_2 powders.

EXIGUI software[31] using the model of $Si_a[S_i]_2$ based on an orthorhombic structure (*Ibam*, ICSD 291210).[11] The preferred orientation of polycrystalline grains was characterized by the texture index (J), texture strength ($J^{1/2}$), and pole figures.

The microstructure and compositions were tested by a field-emission scanning electron microscope (S-4800, Hitachi Ltd., Japan), and a field-emission scanning/transmission electron microscope equipped with an X-ray spectrometer for energy-dispersive spectroscopy (EDS) (Talos F200S G2, ThermoFisher Sci. Inc., USA).

3. RESULTS AND DISCUSSION

3.1. Chemical Purity. 31 elements were analyzed by ICP for the acid-pickled raw materials (S and Si) and the synthesized SiS_2 powders (Figure 3). It showed that the W impurity induced by WC-Co ball-milling was much more difficult to be removed by the acid-pickling process than the Fe induced by Fe ball-milling.[5,28,29] All samples except the Si# (WC-Co-ball-milled Si powder) had a low content of element impurity (<690 ppm; w/o Na) and a low total impurity content (~99.95 wt % purity; w/o Na). The acid-pickled Si, the synthesized SiS_2_LUT, SiS_2_HU, and SiS_2_HUT had a relatively high content of Na, as a result of a high content of total impurity content. It might come from utensils, containers, or test errors. More studies are underway.

3.2. Phase Purity and Crystal Structure. The acid-pickled S was indexed to the orthorhombic α-S_8(s) with annular molecules (*FdddZ*, no. 70; ICSD 63083) (Figure 4a). At low temperatures (<432 K), the prevailing S-molecular species were those of cycloocta-S, cyclo-S_8, and small molecules (from S_2 to S_8) with minimal and negligible quantities identified in the solid, liquid, and gaseous phases.[34−36] When heated, it will transform to various forms of polymeric S_n-chains, catena or mixed cyclo-linear, for example, monoclinic β-S_8(s) at 369 K, monoclinic λ-S(l) with long-chain molecules near its melting point ($T_{m.p.}$@S = 388.36 K), and amorphous μ-S(l) at 432−433 K. Last, it would turn into a gas at its boiling point ($T_{b.p.}$@S = 717.75 K).[23,32] The acid-pickled Si was indexed to the cubic phase ($Fd\bar{3}mS$, no. 227; ICSD 51688). The S and Si started to react below 628−663 K.[22,23,32−37]

$$S(l) \xrightarrow{1023\ K/2.57\ MPa\ -\ 1073\ K/3.83\ MPa} S(g) \quad (2)$$

$$Si(s) + 2S(l) \xrightarrow{1023\ K/2.57\ MPa\ -\ 1073\ K/3.83\ MPa} SiS_2(s) \quad (3)$$

$$Si(s) + 2S(g) \xrightarrow{1023\ K/2.57\ MPa\ -\ 1073\ K/3.83\ MPa} SiS_2(s) \quad (4)$$

Two of the eqs 2−4 are independent.

XRD patterns of the synthesized SiS_2 samples could be indexed to pure (100 wt %) orthorhombic SiS_2 phases except for SiS_2_HU. The SiS_2_HU contained a small amount of residual α-S_8, which was easily removed by benzene. All patterns were almost the same, including background, peak positions, shapes, and relative intensities. However, these relative intensities were obviously different with those deduced from the ICSD 291210 (*Ibam*, no. 72).[11] Thus, the preferred orientation correction[31,38,39] was introduced into the Rietveld refinement of the SiS_2_HUT sample (Figure 4b). The refinement did not show any anomalies. The fit converged with acceptable goodness-of-fit (χ^2 = 2.62) and agreement indices (R_p = 5.49%, R_{wp} = 8.72%, R_{exp} = 3.34%, and R_F^2 = 9.14%). The obtained structural and thermal parameters are reasonable (Table 1).[11,40]

It showed orthorhombic SiS_2 phases could be synthesized through the boiling/steaming process in a uniform-temperature zone (1023−1073 K, 3 h) and under the corresponding saturated S-vapor pressure ($P_{sat.}$@S = 2.57−3.83 MPa).[34]

The chemical bonds in the orthorhombic SiS_2 are anisotropic. Distorted edge-sharing [SiS_4] tetrahedra link as chains along the *c*-axis (the inset of Figure 4b). There is very rigid covalent bonding between the tetrahedra in the direction [0 0 1], while there is weak ionic and van der Waals bonding with an "open"

https://doi.org/10.1021/acsomega.2c01725
ACS Omega 2022, 7, 22500−22510

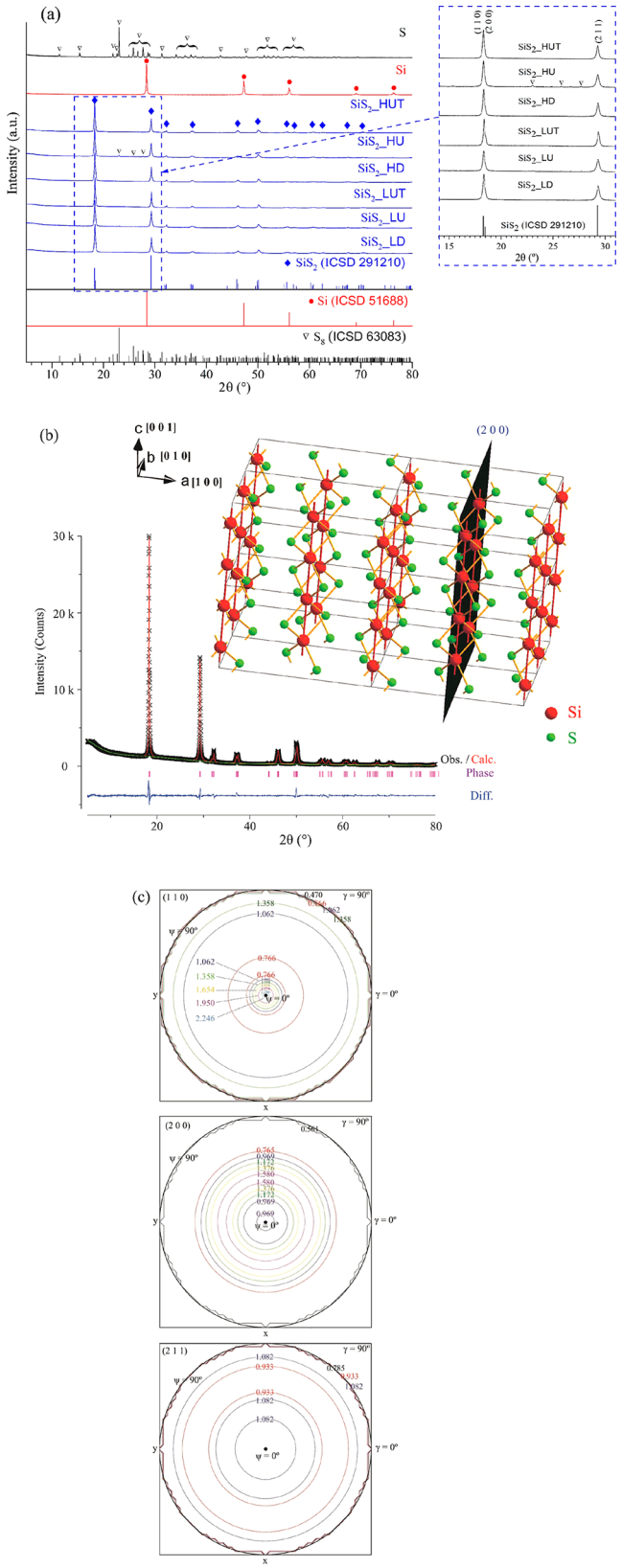

Figure 4. (a) XRD patterns of the acid-pickled raw materials (S and Si) and the synthesized SiS_2 powders; (b) Final observed, calculated, and difference profiles of the structure for SiS_2_HUT via Rietveld refinement. The inset is the crystal-cell view in the direction [0 1 0]; (c) pole figures for the first three allowed reflections in SiS_2_HUT, that is, (1 1 0), (2 0 0), and (2 1 1).

structure in the other two directions (a and b).[11,40] From the structure refinement with spherical harmonics function, the allowed eighth-order harmonic coefficients (C_l^{mm}) were calculated. They are related to the reflection-intensity correction factors that describe the texture effects. Then, the texture index (J) and texture strength ($J^{1/2}$) which depends on C_l^{mm} were concluded, that is, $J = 1.6149$ (*c.f.* $J = 1$ for random, otherwise $J > 1$; $J = \infty$ for a single crystal) and $J^{1/2} = 1.2708$.

Pole figures present that the statistical orientation distribution of the plane normals from a particular set of planes gives a mapping of the probability of possible grain orientations.[31,38,39] Figure 4c showed pole figures constructed for the first three allowed reflections in orthorhombic SiS_2 with the comparatively low symmetry, that is, (1 1 0), (2 0 0), and (2 1 1), in which the relative populations of planes in various orientations were proportional to the numbers (represent relative intensities of the diffraction signal) against the contour lines.

It confirmed that the synthesized orthorhombic SiS_2 powders presented polycrystalline alignment with oriented [0 0 1] texture microstructures.

3.3. Microstructure (SEM and TEM/EDS). Scanning electron microscopy/transmission electron microscopy (SEM/TEM) images and EDS mappings of the acid-pickled Si and the synthesized SiS_2 powders are shown in Figure 5i–viii. The length (L), diameter (D), and length-to-diameter ratio (L/D) of Si and SiS_2 rods/particles from SEM image analysis are shown in Figure 6.

The S was kept in the liquid and gaseous states in this work thus the initial size (as opposed to chemical purity) needs not be too concerned.

The acid-pickled Si has a small particle size and a uniform particle size distribution of 3.3 ± 0.9 μm (Figures 5i and 6). It means that the Fe-based medium for ball-milling Si powder is highly effective for decreasing particle size and maintaining a high chemical purity (by post-acid-pickling).[5,28,29]

SiS_2 particles prepared with the quartz tubes at a down (D) site (solid–liquid boiling process, Figure 1a), whether at low (L) or high (H) temperature (1023/1073 K), have irregular shapes and feature a little rod-like, such as SiS_2_LD (Figure 5ii) and SiS_2_HD (Figure 5v). Their mean particle diameters are 3.8 ± 1.2 μm and 4.9 ± 1.3 μm, respectively (Figure 6). The forced-convective S-liquid stirred constantly the solid Si/SiS_2 and destroyed the rods (see Section 3.4).

SiS_2 particles prepared with the quartz tubes at an up (U) site (solid–gas steaming process, Figure 1b), whether at low (L) or high (H) temperature (1023/1073 K), have rod-like shapes and feature very little irregular, such as SiS_2_LU (Figure 5iii), SiS_2_LUT (Figure 5iv), SiS_2_HU (Figure 5vi), and SiS_2_HUT (Figure 5vii and viii). The solid–gas steaming process provided a more stable growth environment for the SiS_2 rods (see Section 3.4). Their mean particle sizes (length/diameter) are 13.4 ± 4.5/3.8 ± 0.9 μm for SiS_2_LU, 12.9 ± 3.0/3.2 ± 0.6 μm for SiS_2_LUT, 16.0 ± 5.4/3.9 ± 0.9 μm for SiS_2_HU, and 16.8 ± 5.0/4.5 ± 1.3 μm for SiS_2_HUT, respectively. The corresponding length-to-diameter (L/D) ratios are 3.5, 4.0, 4.1, and 3.7, respectively. The length increases 19–30% with preparation-temperature increasing, while the diameter increases by varying degrees. Thus, the resulting L/D values change a little (Figure 6).

The TEM imagine and EDS mappings of SiS_2_HUT (Figure 5viii) showed a homogeneous elemental distribution of S and Si in SiS_2 rods. No impurities were detected.

https://doi.org/10.1021/acsomega.2c01725
ACS Omega 2022, 7, 22500–22510

Table 1. Rietveld Refinement Parameters and Results of the Structure for the SiS_2_HUT Sample

ions	type	Wyckoff	x	y	z	Occ.	U_{iso} (Å^2)
Si^{4+}	Si1	4*a*	0.0000	0.0000	0.2500	1.0	0.029(1)
S^{2-}	S1	8*j*	0.1178(2)	0.2078(4)	0.0000	1.0	0.035(1)
χ^2	R_p	R_{wp}	R_{exp}	R_F^2	N_{obs}	$N_{constr.}$	
2.62	5.49%	8.72%	3.34%	9.14%	5769	0	

Space group: *Ibam* (no. 72); orthorhombic; $Z = 4$; $M_r = 92.2175$; $\rho_{cal.} = 2.0400$ g·cm^{-3}. $a = 9.6152(6)$ Å; $b = 5.6224(2)$ Å; $c = 5.5543(4)$ Å; $\alpha = \beta = \gamma = 90°$; $V = 300.264(16)$ Å^3.

Comparing the images of SiS_2_LU (Figure 5iii) with SiS_2_LUT (Figure 5iv) and SiS_2_HU (Figure 5vi) with SiS_2_HUT (Figure 5vii), they showed that the residual S could be effectively eliminated through benzene treatment. In addition, the benzene could modify the microstructure and dispersion of SiS_2 particles.

Specially, Figure 6 showed that particle diameters of both Si and SiS_2 powders were in the same order of magnitude, meaning that the particle diameter of a SiS_2 particle depended mainly on that of a Si particle. A single Si-particle (rather than several Si-particles) reacted with liquid/gaseous S and then grew into a rod along a preferred direction.

The preferred orientation of orthorhombic SiS_2 has been reported before, such as SiS_2 with a fibrous, a needle-shaped, or a pillar-shaped morphology/structure.[3,13,16] However, so far, there is little explanation for the growth mechanism. Some orthorhombic materials with preferred orientation have also been investigated, such as Bi_2S_3 nanorods[41−43] or nanotubes,[43] Sb_2S_3 nanorods,[44] BiSCl polygonal tubes, BiSI bundle-rods,[45] and so on. Their growth mechanism was explained to be related to the large surface tension of the solution,[42,43] the large surface energy of products,[41] environment pressure,[44] or the inherent structural characteristics of products.[41,42,44,45]

In this work, the orthorhombic SiS_2 powders with an oriented microstructure were prepared through the boiling/steaming process in a uniform-temperature zone (1023−1073 K) and under the saturated S-vapor pressure ($P_{sat.}$@S = 2.57−3.83 MPa). The relatively high pressure is more favorable for the formation of SiS_2-rods in the closed sealed-tube system (which is similar to the hydrothermal one) than that in an open system.[44] The texture had a consequence of the thermal/polycrystalline growth history. The synthesis conditions could affect the macroscopic morphology but could not change the microstructural anisotropy.[45] The intrinsic crystal-structure characteristics, being independent of synthesis conditions, determined the growth orientation of SiS_2 rods. The synthesis temperature depended on the particle size of Si, and its dispersing condition in the melted/gasified S.[20] The latter was no doubt excellent in this work.

According to the Bravais' law, for the orthorhombic SiS_2, the observed crystal faces are parallel to the net planes with the highest reticular densities (or smallest mesh areas), that is, (1 0 0); the greater ones are corresponding to the more important forms. During synthesizing, big SiS_2 grains preferentially grew into rods on (1 0 0) by consuming small grains on (1 1 0)/(2 1 1), which had low reticular densities (or large mesh areas). Moreover, the ratio of length-to-diameter gradually increased. As stated before, most of the Si−S bonds along the *c* axis have the shortest bond-length and strongest bond-energy. The SiS_2 rods grew along [0 0 1] were rather stable thermodynamically and hard to be cleaved once the Si−S chemical bond was formed. The growth along [0 0 1] was intrinsically governed by the highest surface energy of plane (0 0 1).[41]

3.4. Growth Mechanism of SiS_2 Rods. According to eq 1, $NP_{1023\ K} = P_{sat.,\ 1023\ K}$@S = 2.57 MPa (<$P_{ctrl.}$ = 3.83 MPa) and $NP_{1073\ K} = P_{sat.,\ 1073\ K}$@S = 3.83 MPa (= $P_{ctrl.}$). For samples prepared at the down (D) site of quartz tubes, the main process was boiling with a solid−liquid reaction between solid Si and S-liquid, while saturated S-vapor stayed at the up (U) site. For samples prepared at the up (U) site of quartz tubes, the main process was steaming with a gas−solid reaction between solid Si and saturated S-vapor, while S-liquid stayed at the down (D) site (Figure 1).

From the thermodynamics viewpoint, there may exist the following reactions to prepare SiS_2 by an "elemental method", for example, at 1023 K (2.57 MPa)−1073 K (3.83 MPa) in this work.

$$Si(s) + S_2(g) = SiS_2(s),\ \Delta G^0(kJ/mol) = -325.24 + 0.1632T\ (<0, \text{when } T < 1993\ K)^{33} \quad (5)$$

$$2Si(s) + S_2(g) = 2SiS(g),\ \Delta G^0(kJ/mol) = 102.55 - 0.1632T(<0, \text{when } T > 628\ K)^{33} \quad (6)$$

$$SiS_2(s) + Si(s) = 2SiS(g),\ \Delta G^0(kJ/mol) = 395.2 - 0.2646T(<0, \text{when } T > 1494\ K)^{37} \quad (7)$$

$$SiS_2(s) = \frac{1}{2}S_2(g) + SiS(g),\ \Delta G^0(kJ/mol) = 387.7 - 0.2354T(<0, \text{when } T > 1647\ K)^{37} \quad (8)$$

The main reaction to synthesize $SiS_2(s)$ (eq 5) proceeds below 1993 K and the side reaction to SiS(g) (eq 6) starts to proceed when $T > 628$ K.[33] The former dominates because it has a larger Gibbs free-energy (absolute value) than the latter. Besides, the forward reactions in eqs 7 and 8 would be very difficult to happen below 1993 K (also in this work), while the partial pressures of SiS(g) are 10^{-3} atm in eq 7[3,37] and 10^{-5} atm in eq 8, respectively.[3,37] This means, if the SiS(g) was generated via eq 6, it would tend to produce $SiS_2(s)$ and Si(s) as in the backward reaction of eq 7 or react with $S_2(g)$ to form $SiS_2(s)$ as in the backward reaction of eq 8. Therefore, the contribution of SiS(g) in the "elemental method" (as in this work) to synthesize $SiS_2(s)$ can be neglected, which is different from that in a "compound method".[3,13,16−20]

For the Si−S reactions, there is an interface between reacting phases. In order for the reaction to proceed, three paths take place in series—transport of reactants (Si/S) to the interface, reaction at the phase boundary (PB), and transport of product (SiS_2) away from the interface.[46] In addition, the exothermic reactions (eqs 3 and 4) at PB liberate heat (given an adiabatic assumption, e.g., in a uniform-temperature zone in this work), change the boundary temperature and limit the reaction rate (r). Any of these steps may determine the overall reaction rate (r) which depends on the slowest one.

https://doi.org/10.1021/acsomega.2c01725
ACS Omega 2022, 7, 22500−22510

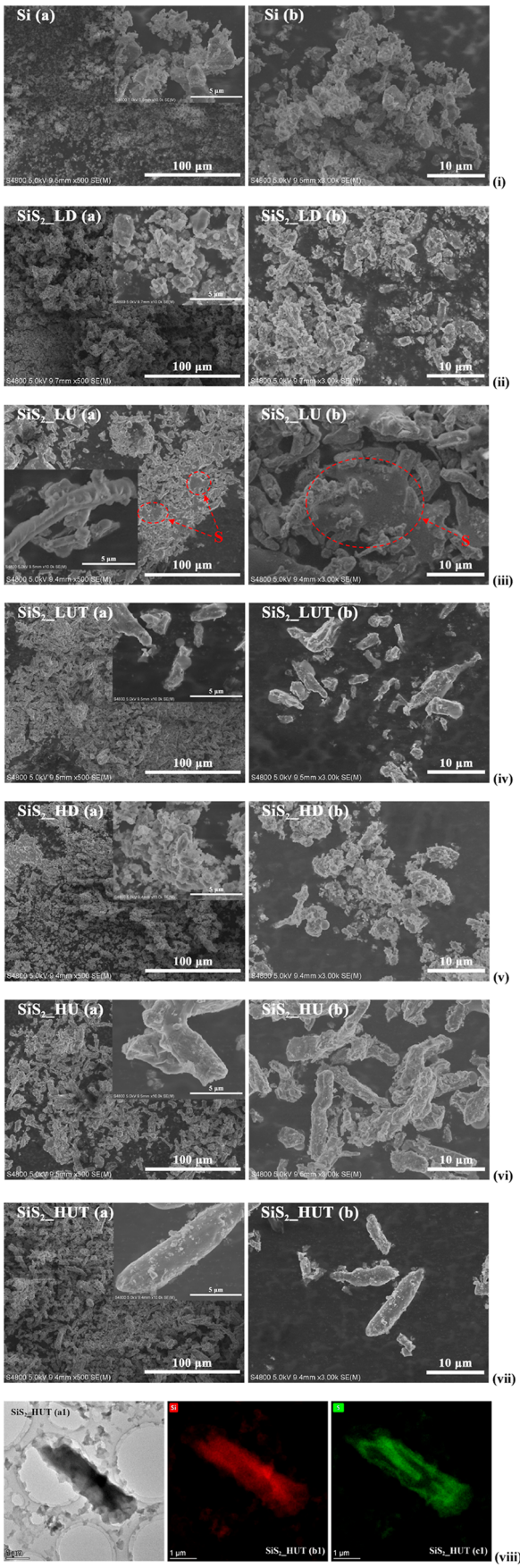

Figure 5. SEM (i–vii), TEM images, and EDS mappings (viii) of Si and the synthesized SiS_2 powders. They are as follows: the Fe-ball-milled and acid-pickled Si [i(a) and i(b)]; the SiS_2 prepared at a low (L) temperature of 1023 K, while the quartz tube was at a down (D) site [ii(a) and ii(b)], at an up (U) site [iii(a) and iii(b)], or at an up (U) site and then treated (T) by benzene [iv(a) and iv(b)]; the SiS_2 prepared at a high (H) temperature of 1073 K, while the quartz tube was at a down (D) site [v(a) and v(b)], at an up (U) site [vi(a) and vi(b)], or at an up (U) site and then treated (T) by benzene [vii(a) and vii(b); viii(a1), viii(b1), and viii(c1)].

Solid–liquid reaction (boiling process; Figure 1a): The process was at 1023 K under 2.57 MPa or at 1073 K under 3.83 MPa. Mass-transport rates of reactants (Si and S) and product (SiS_2) increased greatly through the forced-convection mass-transport step in the S-liquid. The PB reaction proceeded mainly between the solid Si and S-liquid, while the saturated S-vapor stayed nearby (eq 3). Therefore, the dominant factor which determines r was the reaction rate of solid-liquid-PB (r^{s-l}). The PB was fixed by the movement of atoms/molecules across the interface in a way equivalent to the grain growth. In this process, the forced-convective boiling S stirred constantly the solid Si/SiS_2 and destroyed the rods, such as SiS_2_LD (Figure 5ii) and SiS_2_HD (Figure 5v).

Solid–gas reaction (steaming process; Figure 1b): Here, mass-transport rates were governed through the forced-convection mass-transport step in the saturated S-vapor. The PB reaction proceeded mainly between the solid Si and saturated S-vapor, while the S-liquid stayed below (eq 4). The dominant factor which determined r was the reaction rate of solid–gas-PB r^{s-g}. When a single Si-particle (surrounded by S-vapor) acted as a heterogeneous reaction surface, the oriented growth of SiS_2 occurred, such as SiS_2_LU (Figure 5iii), SiS_2_LUT (Figure 5iv), SiS_2_HU (Figure 5vi), and SiS_2_HUT (Figure 5vii and viii).

Then, consider the reactions from the kinetics viewpoint. The calculations of Rau et al.[34−36] concluded that the mean S-atom number per molecule is 3 in the liquid state [i.e., S_3(l)] and 4.7 in the gaseous one [i.e., $S_{4.7}$(g)] in the range of 1023–1073 K. Referring to eqs 3 and 4, the kinetic equations could be expressed as eq 9. The relationship among reaction pressure, concentrations of reactant (S)/product (SiS_2), and reaction time showed in Table 2 and Figure 7. Here, the t refers to time. The a, b, and c are initial ($t = 0$) concentrations of Si(s) (= $[Si]_0$ = 1.23 mol/dm^3), S_3(l) (= $[S_3]_0$), and $S_{4.7}$(g) (= $[S_{4.7}]_0$), respectively ($a \leq 1.5b + 2.35c$). Here, the initial concentration of single S, that is, $[S]_0 = 4.059$ mol/dm^3 = $3b + 4.7c$, while $\delta = 3.3$. The x, $(a - x)$, $(b - ux)$ and $c - ((2-3u)/4.7)x$ are instantaneous ($t = t$) concentrations of SiS_2(s) (= $[SiS_2]$), Si(s) (= [Si]), S_3(l) (= $[S_3]$), and $S_{4.7}$(g) (= $[S_{4.7}]$), respectively ($0 < x < a$). The c values (= $[S_{4.7}]_0$) were calculated by the ideal gas equation under $P_{sat.}@S_{4.7}$.[34] When the reactions went on at 1023 K, the S-vapor pressure in the tube remained constant (= $P_{sat.,\ 1023\ K}@S_{4.7}$ = 2.57 MPa). However, when the reactions completed 82.9% (= 1.02/1.23 × 100%) at 1073 K, the S-vapor pressure became smaller (between 3.03–3.83 MPa) than $P_{sat.,\ 1073\ K}@S_{4.7}$ (= 3.83 MPa) because all the liquid S had been gasified earlier. The amount of S-liquid was the difference between those of the total S and S-vapor.

The $b_{l,\infty}$ and $b_{g,\infty}$ correspond to the amount of residual S_3(l) and $S_{4.7}$(g) when the reactions just finished at the synthesis temperature, respectively. The total residual S, that is, $S_{rest} = b_{l,\infty} + b_{g,\infty} = 3b + 4.7c - a$.

The differential-type kinetic equations are as the following:

https://doi.org/10.1021/acsomega.2c01725
ACS Omega 2022, 7, 22500−22510

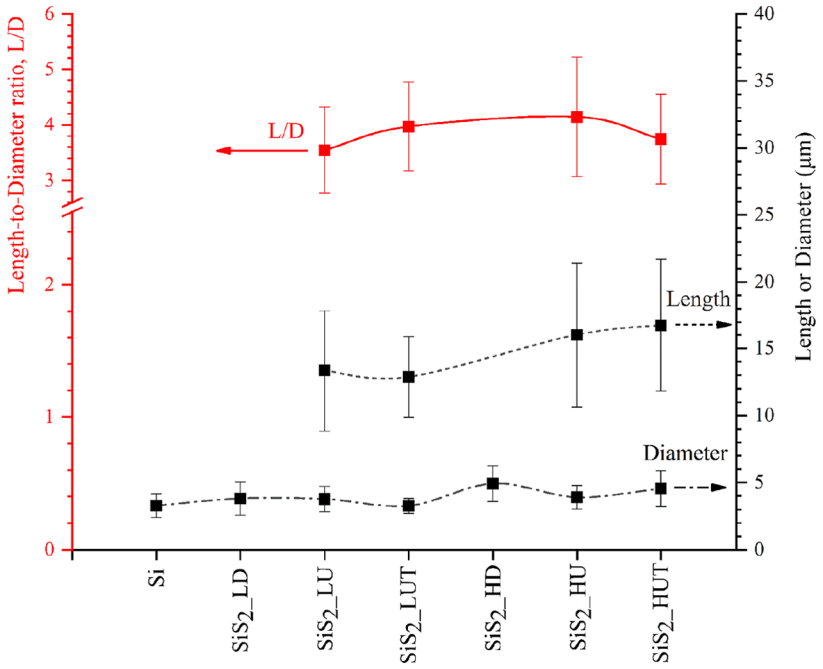

Figure 6. Length (L), diameter (D), and length-to-diameter ratio (L/D) of Si and SiS_2 rods/particles from SEM image analysis.

Table 2. Kinetic Equations and the Relationship between Initial/Final Concentrations ($[C]_i/[C]_f$) of Reactant (S)/Product (SiS_2) and Reaction Time (t)

$$\mathrm{Si(s)} + u\mathrm{S_3(l)} + \left(\frac{2-3u}{4.7}\right)\mathrm{S_{4.7}(g)} \rightarrow \mathrm{SiS_2(s)} \quad (9)$$

$t = 0$	Conc. (mol/dm^3)	a	b	c	0
	$[C]_{i,1023\ K}{}^{s-l}$	1.23	0.880	0.302	0
	$[C]_{i,1023\ K}{}^{s-g}$	1.23	0.880	0.302	0
	$[C]_{i,1073\ K}{}^{s-l}$	1.23	0.680	0.429	0
	$[C]_{i,1073\ K}{}^{s-g}$	1.23	0.680	0.429	0
$t = t$	Conc. (mol/dm^3)	$a - x$	$b - ux$	$\left(c - \frac{2-3u}{4.7}\right)x$	x
	$[C]_{1023\ K}{}^{s-l}$	$1.23 - x$	$0.880 - 2/3x$	0.302	x
	$[C]_{1023\ K}{}^{s-g}$	$1.23 - x$	$0.880 - 2/3x$	0.302	x
	$[C]_{1073\ K}{}^{s-l}$	$1.23 - x$	$0.680 - 2/3x$	0.429	x
	$[C]_{1073\ K}{}^{s-g}$	$1.23 - x$	$0.680 - 2/3x$	0.429	x
$t = \infty$	Conc. (mol/dm^3)	0	$b_{l,\infty}$	$c_{g,\infty}$	a
	$[C]_{f,\ 1023\ K}{}^{s-l}$	0	0.060	0.302	1.23
	$[C]_{f,1023\ K}{}^{s-g}$	0	0.060	0.302	1.23
	$[C]_{f,1073\ K}{}^{s-l}$	0	0.000	0.340	1.23
	$[C]_{f,1073\ K}{}^{s-g}$	0	0.000	0.340	1.23

$$r = \frac{dx}{dt} = \frac{d[SiS_2]}{dt} = -\frac{d[Si]}{dt} = -\frac{d[S_3]}{udt} = -\frac{4.7d[S_{4.7}]}{(2-3u)dt} = k(a-x)^{\alpha}(b-ux)^{\beta}\left[c - \left(\frac{2-3u}{4.7}\right)x\right]^{\gamma},\ a \le \frac{1}{2}\cdot(3b + 4.7c) \text{ and } 0 < x < a \quad (10)$$

where k refers to the rate constant of reaction. $k = k_{SiS_2} = k_{Si} = (1/u)k_{S_3} = (4.7/(2-3u))k_{S_{4.7}}$. The α, β, and γ are the sub-orders of reaction (all > 0). Parallel solid−liquid (eq 3) and solid−gas (eq 4) reactions proceeded simultaneously as the following:

$$r = r^{s-l} + r^{s-g} \quad (11)$$

$$r^{s-l} = k^{s-l}(a_l - x)^{\alpha}(b - ux)^{\beta},\ a_l \le 1.5b \text{ and } 0 < x < a_l \quad (12)$$

$$r^{s-g} = k^{s-g}(a_g - x)^{\alpha}\left[c - \left(\frac{2-3u}{4.7}\right)x\right]^{\gamma},\ a_g \le 2.35c \text{ and } 0 < x < a_g \quad (13)$$

where k^{s-l} and k^{s-g} are the rate constants of the solid−liquid phase-boundary (PB) and solid−gas phase-boundary (PB), respectively. The following superscript symbols have the same meanings. The a_l and a_g correspond to the amount of Si reacted with $S_3(l)$ and $S_{4.7}(g)$, respectively.

For the boiling process to synthesize SiS_2 at 1023/1073 K and a down (D) site in quartz tubes, eq 12 (same as the following eqs 14 and 15) was the primary reaction.

$$r^{s-l}_{1023\ K} = k^{s-l}_{1023\ K}(1.23 - x)^{\alpha}\left(0.880 - \frac{2}{3}x\right)^{\beta},\ 0 < x < 1.23 \quad (14)$$

This was a complete solid−liquid reaction. Where $a_g \rightarrow 0$, $a_l = a = 1.23$ mol/dm^3 and $u = 2/3$. The $[S_{4.7}]$ kept constant ($= c = 0.302$ mol/dm^3) until the end of the reaction. $b = (3.3 \times 1.23 - 4.7 \times 0.302)/3 = 0.880$ mol/dm^3.

$$r^{s-l}_{1073\ K} = k^{s-l}_{1073\ K}(1.23 - x)^{\alpha}\left(0.680 - \frac{2}{3}x\right)^{\beta},\ 0 < x < 1.02 \quad (15)$$

This was an incomplete solid−liquid reaction. Where $a_g \rightarrow 0$, $a_l = a = 1.23$ mol/dm^3 and $u = 2/3$. The $[S_{4.7}]$ kept constant ($= c = 0.429$ mol/dm^3) until 82.9% ($= 1.02/1.23 \times 100\%$) SiS_2 was obtained. $b = (3.3 \times 1.23 - 4.7 \times 0.429)/3 = 0.680$ mol/dm^3. The $S_3(l)$ consumption was 0.680 mol/dm^3 and that of $S_{4.7}(g)$ was 0.089 mol/dm^3 ($= 0.429 - 0.340$ mol/dm^3). In other words, the last 17.1% SiS_2 was synthesized through a solid−gas reaction.

https://doi.org/10.1021/acsomega.2c01725
ACS Omega 2022, 7, 22500−22510

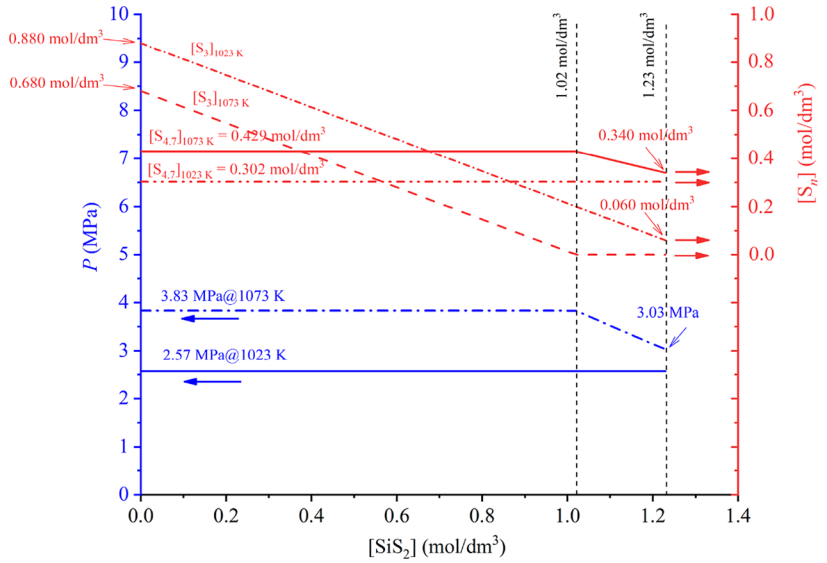

Figure 7. Relationship between reaction pressure and concentrations of reactant (S)/product (SiS_2).

For the steaming process to synthesize SiS_2 at 1023/1073 K and a up (U) site in quartz tubes, eq 13 (same as the following eqs 16 and 17) was the primary reaction.

$$r^{s-g}_{1023\ K} = k^{s-g}_{1023\ K}(1.23 - x)^{\alpha},\ 0 < x < 1.23 \quad (16)$$

This was a complete solid−gas reaction. Where $a_l \to 0$, $a_g = a$ = 1.23 mol/dm^3 and u = 2/3. The $[S_{4.7}]$ kept constant (= c = 0.302 mol/dm^3) until the end of the reaction. The amount of $S_{4.7}$(g) which reacted with Si(s) equals that of the gasified S_3(l), while the latter decreased from 0.880 to 0.060 mol/dm^3.

$$r^{s-g}_{1073\ K} = k^{s-g}_{1073\ K}(1.23 - x)^{\alpha},\ 0 < x < 1.02 \quad (17)$$

This was a complete solid−gas reaction. Where $a_l \to 0$, $a_g = a$ = 1.23 mol/dm^3 and u = 2/3. The $[S_{4.7}]$ kept constant (= c = 0.429 mol/dm^3) until 82.9% (= 1.02/1.23 × 100%) SiS_2 was obtained. The amount of $S_{4.7}$(g) which reacted with Si(s) included that of the gasified S_3(l) (= 0.680 mol/dm^3) and the other $S_{4.7}$(g) consumption (= 0.429−0.340 = 0.089 mol/dm^3). The residual $S_{4.7}$(g) was 0.340 mol/dm^3 and residual S_3(l) was zero.

Comparing eq 14 with 15 and eq 16 with 17, the following equations could be obtained ($0 < x < 1.23$)

$$\frac{r^{s-l}_{1023\ K}}{r^{s-l}_{1073\ K}} = \left(\frac{0.880 - \frac{2}{3}x}{0.680 - \frac{2}{3}x}\right)^{\beta} \times \frac{k^{s-l}_{1023\ K}}{k^{s-l}_{1073\ K}},\ 0 < x < 1.02 \quad (18)$$

$$\frac{r^{s-g}_{1023\ K}}{r^{s-g}_{1073\ K}} = \frac{k^{s-g}_{1023\ K}}{k^{s-g}_{1073\ K}},\ 0 < x < 1.02 \quad (19)$$

Because $(0.880-2/3x)/(0.680-2/3x) > 1$, $\beta > 0$ and the $k^{s-l}_{1023\ K}/k^{s-l}_{1073\ K}$ is slightly less than 1 (according to the Arrhenius rule from the kinetics viewpoint), so $r^{s-l}_{1023\ K}/r^{s-l}_{1073\ K}>1$. The temperature increasing would result in the decreasing of the solid-liquid-PB reaction rate (r^{s-l}) in the boiling process. In other words, the low temperature is beneficial to the boiling process.

Because the $k^{s-g}_{1023\ K}/k^{s-g}_{1073\ K}$ is slightly less than 1 (same as the above), so $r^{s-g}_{1023\ K}/r^{s-g}_{1073\ K}<1$. The temperature increasing would result in the increasing of the solid−gas-PB reaction rate (r^{s-g}) in the steaming process. In other words, the high temperature is beneficial to the steaming process.

To sum up, the synthesis method for SiS_2 in this work is safe (*cf.* dangerous H_2S and CS_2),[3,18,19] economical [*cf.* expensive Al_2S_3 and $(C_2H_5S)_4Si$],[13,18,19] convenient (*cf.* soaking for 150 h,[20] 3 d[10,11] or 7 d[22]; calcining for 70−80 h[6] or 12 d;[10,11] complicated process[6] to eliminate residual S), and feasible with acceptable requirements for facilities and operations.[5]

4. CONCLUSIONS

In this work, the SiS_2 rods were prepared by using the excess sulfur formula either through a solid−liquid boiling process or a solid−gas steaming process.

The relatively high pressure (2.57 MPa@1023 K and 3.83 MPa@1073 K) is more favorable for the formation of SiS_2-rods in the closed sealed-tube system (with a uniform-temperature zone) than that in an open system. The chemical (*c.f.* evaporation) approach using benzene is first used to eliminate residual S to prepare pure SiS_2.

The SiS_2 rods have controllable microstructure and high chemical/phase purity. The optimized synthesis condition can affect the macroscopic morphology but cannot enough change the microstructural anisotropy.

The gaseous SiS is hardly present in this "elemental method" between 1023 and 1073 K which is different with that in a "compound method". The SiS_2 rods were synthesized through solid−liquid/solid−gas reactions among the Si(s), S_3(l), and $S_{4.7}$(g). The low temperature is beneficial to the solid−liquid reaction and the high temperature to the solid−gas reaction.

■ ASSOCIATED CONTENT

Supporting Information

The Supporting Information is available free of charge at https://pubs.acs.org/doi/10.1021/acsomega.2c01725.

Crystallographic data for SiS_2 and further details of the crystal structure investigation may be obtained from Cambridge Crystallographic Data Centre (UK) and inorganic Crystal Structure Database of FIZ Karlsruhe (Germany) on quoting the appropriate ICSD number (SiS_2_1073 K_3.8 MPa, ICSD 2151800, 2022.2.14), DOI: 10.5517/ccdc.csd.cc2b73xm (CIF)

https://doi.org/10.1021/acsomega.2c01725
ACS Omega 2022, 7, 22500−22510

AUTHOR INFORMATION

Corresponding Author

Gang-Qin Shao − *State Key Laboratory of Advanced Technology for Materials Synthesis and Processing, Wuhan University of Technology, Wuhan 430070, China;* orcid.org/0000-0001-6002-5910; Phone: +86 27 87884448; Email: gqshao@whut.edu.cn; Fax: +86 27 87884448

Authors

Meng-Xiang Xie − *State Key Laboratory of Advanced Technology for Materials Synthesis and Processing, Wuhan University of Technology, Wuhan 430070, China*

Ji-Wei Zhang − *State Key Laboratory of Advanced Technology for Materials Synthesis and Processing, Wuhan University of Technology, Wuhan 430070, China*

Yong Zhang − *State Key Laboratory of Advanced Technology for Materials Synthesis and Processing, Wuhan University of Technology, Wuhan 430070, China*

Hou-Ran Wu − *State Key Laboratory of Advanced Technology for Materials Synthesis and Processing, Wuhan University of Technology, Wuhan 430070, China*

Yan-Pei Wang − *State Key Laboratory of Advanced Technology for Materials Synthesis and Processing, Wuhan University of Technology, Wuhan 430070, China*

Wen-Hao Wang − *State Key Laboratory of Advanced Technology for Materials Synthesis and Processing, Wuhan University of Technology, Wuhan 430070, China*

Complete contact information is available at: https://pubs.acs.org/10.1021/acsomega.2c01725

Author Contributions

M.-X. Xie and J.-W. Zhang: investigation, data analysis, and writing-original draft. Y. Zhang, H.-R. Wu, Y.-P. Wang, and W.-H. Wang: data validation. G.-Q. Shao: review and editing, conceptualization, supervision, and project administration. All authors have given approval to the final version of the manuscript.

Notes

The authors declare no competing financial interest.

ACKNOWLEDGMENTS

Authors acknowledge gratefully Prof. J.-X. Mi in Xiamen University and Prof. B.-L. Wu in Guilin University of Technology for their helpful advice to the polycrystalline structure analysis.

REFERENCES

(1) Wu, F.; Fitzhugh, W.; Ye, L.-H.; Ning, J.-X.; Li, X. Advanced sulfide solid electrolyte by core-shell structural design. *Nat. Commun.* **2018**, *9*, 4037.

(2) Zhao, R.; Hu, G.; Kmiec, S.; Gebhardt, R.; Whale, A.; Wheaton, J.; Martin, S. W. New amorphous oxy-sulfide solid electrolyte material: anion exchange, electrochemical properties, and lithium dendrite suppression *via in situ* interfacial modification. *ACS Appl. Mater. Interfaces* **2021**, *13*, 26841−26852.

(3) Suzuki, R. O.; Yashima, Y.; Kaneko, T.; Ahmadi, E.; Kikuchi, T.; Watanabe, T.; Nogami, G. Synthesis of silicon sulfide by using CS_2 gas. *Metall. Mater. Trans. B* **2021**, *52*, 1379−1391.

(4) Bai, Y.; Zhao, Y.; Li, W.; Meng, L.; Bai, Y.; Chen, G. Organic-inorganic multi-scale enhanced interfacial engineering of sulfide solid electrolyte in Li-S battery. *Chem. Eng. J.* **2020**, *396*, 125334.

(5) Zhang, Y.; Xie, M.-X.; Zhang, W.; Yan, J.-L.; Shao, G.-Q. Synthesis and purification of SiS_2 and Li_2S for $Li_{9.54}Si_{1.74}P_{1.44}S_{11.7}Cl_{0.3}$ solid electrolyte in lithium-ion batteries. *Mater. Lett.* **2020**, *266*, 127508.

(6) Bayko, D. P.; Kmiec, S.; Martin, S. W. Method of making high quality silicon sulfide. U.S. Patent 20,210,292,173 A1, 2020.

(7) Bai, Y.; Zhao, Y.; Li, W.; Meng, L.; Bai, Y.; Chen, G. New insight for solid sulfide electrolytes LSiPSI by using Si/P/S as the raw materials and I doping. *ACS Sustainable Chem. Eng.* **2019**, *7*, 12930−12937.

(8) Kim, K.-H.; Martin, S. W. Structures and properties of oxygen-substituted $Li_{10}SiP_2S_{12-x}O_x$ solid-state electrolytes. *Chem. Mater.* **2019**, *31*, 3984−3991.

(9) Zhao, R.; Kmiec, S.; Hu, G.; Martin, S. W. Lithium thiosilicophosphate glassy solid electrolytes synthesized by high-energy ball-milling and melt-quenching: improved suppression of lithium dendrite growth by Si doping. *ACS Appl. Mater. Interfaces* **2019**, *12*, 2327−2337.

(10) Evers, J.; Möckl, L.; Oehlinger, G.; Köppe, R.; Schnöckel, H.; Barkalov, O.; Medvedev, S.; Naumov, P. More than 50 years after its discovery in SiO_2 octahedral coordination has also been established in SiS_2 at high pressure. *Inorg. Chem.* **2017**, *56*, 372−377.

(11) Evers, J.; Mayer, P.; Möckl, L.; Oehlinger, G.; Köppe, R.; Schnöckel, H. Two high-pressure phases of SiS_2 as missing links between the extremes of only edge-sharing and only corner-sharing tetrahedra. *Inorg. Chem.* **2015**, *54*, 1240−1253.

(12) Dive, A.; Benmore, C.; Wilding, M.; Martin, S. W.; Beckman, S.; Banerjee, S. Molecular dynamics modeling of the structure and Na^+-Ion transport in Na_2S + SiS_2 glassy electrolytes. *J. Phys. Chem. B* **2018**, *122*, 7597−7608.

(13) Peters, J.; Krebs, B. Silicon disulphide and silicon diselenide: a reinvestigation. *Acta Crystallogr.* **1982**, *38*, 1270−1272.

(14) Silverman, M. S.; Soulen, J. R. High pressure synthesis of new silicon sulfides. *Inorg. Chem.* **1965**, *4*, 129−130.

(15) Prewitt, C. T.; Young, H. S. Germanium and silicon disulfides: structure and synthesis. *Science* **1965**, *149*, 535−537.

(16) Zintl, G.; Loosen, K. Siliciumdisulfid, ein anorganischer Faserstoff mit Kettenmolekülen. *Z. Phys. Chem.* **1935**, *174A*, 301−311.

(17) Büssem, W.; Fischer, H.; Gruner, E. Die struktur des siliciumdisulfids. *Sci. Nat.* **1935**, *23*, 740.

(18) Tiede, E.; Thimann, M. Pyrogene Darstellung einiger Sulfide, insbesondere von Siliciumdisulfid und Borsulfid, mit Hilfe von Aluminiumsulfid. *Ber. Dtsch. Chem. Ges.* **1926**, *59*, 1703−1706.

(19) Haas, A. The Chemistry of Silicon-Sulfur Compounds. *Angew. Chem., Int. Ed.* **1965**, *4*, 1014−1023.

(20) Yamamoto, K.; Ikeda, N. Method of manufacturing silicon sulfide. U.S. Patent 5,843,391 A, 1997.

(21) Wu, W.-B.; Shu, X.-M. Double-temperature-zone gas-solid synthesis process of silicon disulfide. CN 113461014 A, 2021.

(22) Dolotko, O.; Gupta, S.; Kobayashi, T.; McDonald, E.; Hlova, I.; Majzoub, E.; Balema, V. P.; Pruski, M.; Pecharsky, V. K. Mechanochemical reactions and hydrogen storage capacities in MBH_4-SiS_2 systems (M = Li or Na). *Int. J. Hydrogen Energy* **2019**, *44*, 7381−7391.

(23) Okamoto, H. S-Si (sulfur-silicon). *J. Phase Equilib. Diffus.* **2008**, *29*, 472.

(24) Babcock, C. L.; Barber, S. W.; Fajans, K. Coexisting structures in vitreous silica. *Ind. Eng. Chem.* **1954**, *46*, 161−166.

(25) Dawihl, W.; Rix, W. Über die festigkeitssteigerung von quarzglas durch temperaturerhöhung. *Z. Phys.* **1939**, *112*, 654−666.

(26) Voigt, M.; Klaumünzer, M.; Thiem, H.; Peukert, W. Detailed analysis of the growth kinetics of zno nanorods in methanol. *J. Phys. Chem. C* **2010**, *114*, 6243−6249.

(27) Fischli, D.; Enders, F.; Boldt, K. Kinetically driven cadmium chalcogenide nanorod growth fed by local cluster aggregates. *J. Phys. Chem. C* **2020**, *124*, 12774−12783.

(28) Zhang, Y. Preparation and lithium-ionic conduction mechanism of novel solid sulfide electrolyte. Master Dissertation, Wuhan University of Technology, Wuhan, Hubei, China, 2020.

(29) Shao, G.-Q.; Xie, M.-X.; Zhang, J.-W.; Wu, H.-R.; Wang, Y.-P.; Wang, W.-H. The silicon disulfide and preparation method. CN 114538448 A, 2022.
(30) Wang, R.; Shen, B.; Sun, H.; Zhao, J. Measurement and correlation of the solubilities of sulfur S_8 in 10 solvents. *J. Chem. Eng. Data* **2018**, *63*, 553−558.
(31) Larson, A. C.; Dreele, R. B. V. *General structure analysis system (GSAS). Report LAUR 86-748, Los Alamos, New Mexico*; Los Alamos National Laboratory: USA, 2004.
(32) Odin, I. N.; Ivanov, V. A.; Petrovskii, A. Y.; Kozlovskii, V. F.; Rezvanov, R. R. P_{TOT}-*T*-*X* diagram of the Si-Se system and homogeneity ranges of silicon chalcogenides from tensimetric data. *Zh. Neorg. Khim.* **2000**, *45*, 98−102.
(33) Rosenqvist, T.; Tungesvik, K. Thermodynamics of silicon sulphides and zinc sulphide. *Trans. Faraday Soc.* **1971**, *67*, 2945−2951.
(34) Rau, H.; Kutty, T. R. N.; Guedes De Carvalho, J. R. F. High temperature saturated vapour pressure of sulphur and the estimation of its critical quantities. *J. Chem. Thermodyn.* **1973**, *5*, 291−302.
(35) Rau, H.; Kutty, T. R. N.; Guedes De Carvalho, J. R. F. Thermodynamics of sulphur vapour. *J. Chem. Thermodyn.* **1973**, *5*, 833−844.
(36) Ferreira, A. G. M.; Lobo, L. Q. The low-pressure phase diagram of sulfur. *J. Chem. Thermodyn.* **2011**, *43*, 95−104.
(37) O'hare, P. A. G. Inorganic chalcogenides: high-tech materials, low-tech thermodynamics. *J. Chem. Thermodyn.* **1987**, *19*, 675−701.
(38) Von Dreele, R. B. Quantitative texture analysis by rietveld refinement. *J. Appl. Crystallogr.* **1997**, *30*, 517−525.
(39) Bunge, H.-J. Expansion of Orientation Distribution Functions in Series of Generalized Spherical Harmonics. *Texture analysis in materials science: mathematical methods*, 1st ed.; Butterworth & Co: London, 1982; pp 47−118.
(40) Xie, M.-X.; Zhang, J.-W.; Zhang, Y.; Wu, H.-R.; Wang, Y.-P.; Wang, W.-H.; Shao, G.-Q. *SiS_2_1073 K_3.8 MPa, ICSD 2151800*; ICSD Commun, 2022.2.14.
(41) Wang, Y.; Chen, J.; Wang, P.; Chen, L.; Chen, Y.-B.; Wu, L.-M. Syntheses, Growth Mechanism, and Optical Properties of [001] Growing Bi2S3 Nanorods. *J. Phys. Chem. C* **2009**, *113*, 16009−16014.
(42) Ge, Z.-H.; Zhang, B.-P.; Shang, P.-P.; Li, J.-F. Control of anisotropic electrical transport property of Bi2S3 thermoelectric polycrystals. *J. Mater. Chem.* **2011**, *21*, 9194−9200.
(43) Liu, Y.; Miao, H.-Y.; Tan, G.-Q.; Zhu, G.-Q. Effect of reaction solvents on morphology of Bi_2S_3 powders. *Chin. J. Inorg. Chem.* **2008**, *24*, 1772−1776.
(44) Yang, J.; Zeng, J.-H.; Yu, S.-H.; Yang, L.; Zhang, Y.-H.; Qian, Y.-T. Pressure-controlled fabrication of stibnite nanorods by the solvothermal decomposition of a simple single-source precursor. *Chem. Mater.* **2000**, *12*, 2924−2929.
(45) Zhu, L.; Xie, Y.; Zheng, X.; Yin, X.; Tian, X. Growth of compound Bi^{III}-VI^{A}-VII^{A} crystals with special morphologies under mild conditions. *Inorg. Chem.* **2002**, *41*, 4560−4566.
(46) Kingery, W. D.; Bowen, H. K.; Uhlmann, D. R. *Introduction to ceramics*, 2nd ed.; Academic Press: John WiJey & Sons, Inc., 1976; pp 381−413.

https://doi.org/10.1021/acsomega.2c01725
ACS Omega 2022, 7, 22500−22510